

Symbiotic nutrient cycling enables the long-term survival of Aiptasia in the absence of heterotrophic food sources

Nils Rådecker^{1*}, Anders Meibom^{1,2}

¹ Laboratory for Biological Geochemistry, School of Architecture, Civil and Environmental Engineering, École Polytechnique Fédérale de Lausanne (EPFL), Lausanne, Switzerland

² Center for Advanced Surface Analysis, Institute of Earth Sciences, University of Lausanne, Lausanne, Switzerland

* to whom correspondence should be addressed: nils.radecker@epfl.ch

ORCID iDs

Nils Rådecker: [0000-0002-2387-8567](https://orcid.org/0000-0002-2387-8567)

Anders Meibom: [0000-0002-4542-2819](https://orcid.org/0000-0002-4542-2819)

Keywords

Aiptasia | heterotrophy | NanoSIMS | nitrogen limitation | photosymbiosis | Symbiodiniaceae

Author contributions

N.R. conceived and conducted the experiment and performed the sample and data analysis. N.R. and A.M. wrote and revised the manuscript.

Conflict of interest

The authors declare no competing interests.

Funding

N.R. and A.M. are supported by the Swiss National Science Foundation, grants 200021_179092 and 205321_212614

Data availability

All associated data [and scripts](#) are available at zenodo.org.

Abstract

Phototrophic Cnidaria are mixotrophic organisms that can complement their heterotrophic diet with nutrients assimilated by their algal endosymbionts. Metabolic models suggest that the translocation of photosynthates and their derivatives from the algae may be sufficient to cover the metabolic energy demands of the host. However, the importance of heterotrophy to the nutritional budget of these holobionts remains unclear. Here, we report on the long-term survival of the photosymbiotic anemone Aiptasia in the absence of heterotrophic food sources. Following one year of heterotrophic starvation, these anemones remained fully viable but showed an 85 % reduction in biomass compared to their regularly fed counterparts. This shrinking was accompanied by a reduction in host protein content and algal density, indicative of severe nitrogen limitation. Nonetheless, isotopic labeling experiments combined with NanoSIMS imaging revealed that the contribution of algal-derived nutrients to the host metabolism remained unaffected due to an increase in algal photosynthesis and more efficient carbon translocation. Taken together, our results suggest that, on a one-year timescale, heterotrophic feeding is not essential to fulfilling the energy requirements of the holobiont. But, while symbiotic nutrient cycling effectively retains carbon in the holobiont over long time scales, our data suggest that heterotrophic feeding is a critical source of nitrogen required for holobiont growth under oligotrophic conditions.

43 Introduction

44 Photosymbiotic Cnidaria, such as corals and anemones, dominate shallow hard-bottom substrates in the
45 oligotrophic tropical ocean (Pandolfi 2002). The key to their evolutionary and ecological success under these
46 conditions lies in their association with endosymbiotic algae of the family Symbiodiniaceae (Stanley 2006;
47 Stanley and van de Schootbrugge 2009). Efficient nutrient exchange in these symbioses couples the
48 heterotrophic metabolism of the host with the autotrophic metabolism of their algal symbionts (Yellowlees et
49 al. 2008; Cunning et al. 2017). Consequently, photosymbiotic Cnidaria are considered mixotrophic as they can
50 acquire nutrients via heterotrophy and autotrophy alike (Fox et al. 2018; Radice et al. 2019). Under
51 oligotrophic conditions, this confers an ecological advantage that enables these animals to outcompete other
52 benthic organisms restricted to either heterotrophic or autotrophic nutrient sources (Muscatine and Porter
53 1977; McCook 2001).

54 In the stable symbiosis, the algal symbionts translocate a large proportion of their photosynthates in the form
55 of sugars and sterols to their host (Falkowski et al. 1984; Burriesci et al. 2012; Tremblay et al. 2014; Hambleton
56 et al. 2019). This carbon translocation fuels the host metabolism and may be sufficient to cover the host's
57 energy demand under optimal environmental conditions (Davies 1984; Rinkevich 1989; Tremblay et al. 2012).
58 The translocated photosynthates have been referred to as 'junk food' because their low nitrogen content limits
59 their potential for anabolic incorporation (Falkowski et al. 1984; Dubinsky and Jokiel 1994). Hence, the
60 utilization of photosynthates by both symbiotic partners depends, in part, on their access to inorganic nitrogen
61 sources from the surrounding seawater (Davies 1984; Morris et al. 2019; Rådecker et al. 2021). However,
62 under the oligotrophic conditions that prevail in the tropical ocean inorganic nitrogen availability is limited
63 (O'Neil and Capone 2008).

64 In contrast, heterotrophic nutrient sources have a proportionally higher nitrogen content that enables efficient
65 anabolic assimilation (Hughes et al. 2010). There is ample evidence demonstrating the nutritional benefits of
66 heterotrophic feeding, e.g., in the form of organic nitrogen or vitamins for both symbiotic partners (Goreau et
67 al. 1971; Porter 1976; Houlbrèque and Ferrier-Pagès 2009). For example, high rates of heterotrophic feeding
68 seem to enable corals to compensate for reduced algal-derived nutrient availability during bleaching; i.e., the
69 stress-induced breakdown of the cnidarian-algal symbiosis (Grottoli et al. 2006; Anthony et al. 2009). However,
70 as our understanding of potential prey dynamics (e.g., zooplankton abundance) and cnidarian grazing on coral
71 reefs remains limited (Lowe and Falter 2015), the importance of heterotrophic nutrients for sustaining the
72 stable cnidarian-algal symbiosis is less clear.

73 Here, we performed a starvation experiment using the photosymbiotic sea anemone *Aiptasia* to study the role
74 of heterotrophic nutrient acquisition in symbiosis. For this, we reared *Aiptasia* for one year in the absence of
75 any heterotrophic nutrient sources. This permitted us to examine the effects of heterotrophic starvation on
76 the symbiosis in light of the underlying carbon and nitrogen cycling and explore the limits of autotrophic
77 nutrient acquisition in the photosymbiotic Cnidaria.

78 Material & Methods

79 *Animal husbandry & experimental design*

80 The experiments and measurements were performed on the photosymbiotic cnidarian model organism
81 *Aiptasia*, i.e., *Exaiptasia diaphana* (Puntin et al. 2022). We used the clonal host line CC7 with its native algal
82 symbiont community dominated by the *Symbiodinium linucheae* strain SSA01 (Sunagawa et al. 2009;
83 Grawunder et al. 2015). Animal cultures were reared in 2 L acrylic food containers filled with artificial seawater
84 (35 PSU, Pro-Reef, Tropic Marin, Switzerland). Artificial seawater was freshly prepared in the dark to minimize
85 any potential microbial contamination. Culture stocks were kept at a constant temperature of 20°C under a
86 12 h: 12 h light-dark cycle (photosynthetic active radiation = 50 $\mu\text{E m}^{-2} \text{s}^{-1}$) using an Algaetron 230 incubator
87 (Photo System Instruments, Czech Republic). Animals were fed once a week with freshly hatched *Artemia*
88 *salina* nauplii (Sanders GSLA, USA) followed by a complete water exchange and removal of biofilms.

89 For the experiment, all animals were reared under the same conditions as outlined above for one year.
90 However, while half of the animals (two culture containers with five animals each) were fed weekly with
91 *Artemia* nauplii (regularly fed control), the other half (two culture containers with five animals each) was
92 reared in the absence of any food sources (heterotrophically starved). Apart from this, all culturing parameters
93 were kept identical, including the weekly cleaning and water exchange. Pedal lacerates of *Aiptasia* were
94 continuously removed to avoid experimental biases due to differences in asexual reproduction and resulting
95 densities of animal populations.

96 *Phenotypic characterization*

97 Following the one-year experiment, treatment responses were recorded. First, photos of representative
98 phenotypes for each of the treatments were taken with an OM-1 camera and a 60 mm f2.8 macro-objective
99 (OM System, Japan) using identical illumination and exposure settings. Then, three animals were collected
100 from each treatment group, transferred to a pre-weighed 1.5 mL Eppendorf tube, and homogenized in 500 μ L
101 Milli-Q water using a PT1200E immersion dispenser (Kinematica, Switzerland).

102 Host and algal symbiont fractions were immediately separated by centrifugation (3000 g, 3 min, sufficient to
103 remove > 95 % of algal symbionts from the supernatant) and the host supernatant was transferred into a new
104 pre-weighed 1.5 mL tube, flash-frozen in liquid nitrogen, and stored at -20°C for later analysis. The algal
105 symbiont pellet was resuspended in 500 μ L Milli-Q water and rinsed by one additional centrifugation and
106 resuspension step. Algal symbiont concentrations were quantified in three technical replicates per sample
107 based on cell shape and chlorophyll autofluorescence using a CellDrop cell counter (DeNovix, USA). The
108 protein content in the defrosted host supernatant was quantified in three technical replicates using the Pierce
109 Rapid Gold BCA Protein Assay Kit (Thermo Scientific, USA) according to the manufacturer's instructions. Algal
110 concentrations and host protein content were extrapolated to the initial sample volume and normalized to
111 holobiont biomass. Holobiont biomass was approximated as dry weight. For this, host and symbiont fractions
112 were dried at 45°C until the weight was stable and the initial weight of empty tubes was subtracted from the
113 final weight. The weight of host and symbiont fractions was corrected for aliquots taken for sample
114 measurements to approximate the dry weight of the holobiont as a whole, i.e., host + symbiont fraction.

115 *Isotope labeling & sample processing*

116 To study treatment effects on symbiotic interactions, we quantified inorganic carbon and nitrogen assimilation
117 and translocation in the symbiosis. For this, three animals from each treatment were transferred to 50 mL
118 glass vials. For isotopic labeling, vials were filled with minimal artificial seawater medium (35 PSU, pH 8.1,
119 355.6 mM NaCl, 46.2 mM MgCl₂, 10.8 mM Na₂SO₄, 9.0 mM CaCl₂, 7.9 mM KCl; (Harrison et al. 1980))
120 containing 2.5 mM NaH¹³CO₃ and 10 μ M ¹⁵NH₄Cl. In addition, one additional animal per treatment was
121 transferred into a vial filled with minimal artificial seawater medium without heavy isotope tracers to serve as
122 unlabeled controls for NanoSIMS measurements. Animals were incubated for 6 h in the light at their regular
123 culture conditions before being transferred to a fixative solution (2.5 % glutaraldehyde and 1 %
124 paraformaldehyde in 0.1 M Sorensen's phosphate buffer). Samples were fixed for 1 h at room temperature
125 followed by 24 h at 4°C before being stored in a preservative solution (1 % paraformaldehyde in 0.1 M
126 Sorensen's phosphate buffer) at 4 °C until further processing. Within four days of fixation, samples were
127 dissected and individual tentacles were processed for resin embedding. Following secondary fixation in 1 %
128 OsO₄ for 1 h, samples were rinsed (3 x MiliQ for 10 min) and dehydrated in a series of increasing ethanol
129 concentrations (30 % for 10 min, 50 % for 10 min, 2 x 70 % for 10 min, 3 x 90 % for 10 min, and 3 x 100 % for
130 10 min) before being transferred to acetone (100 % for 10 min). Dehydrated samples were gradually infiltrated
131 with SPURR resin (Electron Microscopy Sciences, USA) at increasing concentrations (25 % for 30 min, 50 % for
132 30 min, 75 % for 1 h, and 100 % overnight) and the resin was polymerized at 65°C for 48 h. Embedded samples
133 were cut into semi-thin sections (200 nm) using an Ultracut E ultramicrotome (Leica Microsystems, Germany)
134 and transferred onto glow-discharged silicon wafers.

135 *Electron microscopy and NanoSIMS imaging*

136 For scanning electron microscopy (SEM), sections were stained with uranyl acetate (1% for 10 min), followed
137 by Reynolds lead citrate solution (10 min). Images of tentacle of sections were taken on a GeminiSEM 500 field
138 emission scanning electron microscope (Zeiss) at 3 kV with an aperture size of 30 μm , and a working distance
139 of 2.8 mm, using the energy selective backscatter detector (EsB; ZEISS) with the filter-grid set at 121 V. For
140 NanoSIMS imaging, sections on wafers were sputter-coated with a 12 nm gold layer using an EM SCD050 (Leica
141 Microsystems) and the samples were analyzed with a NanoSIMS 50L instrument (Hoppe et al. 2013). To
142 remove the metal coating, target sample areas were pre-sputtered for 5 min with a primary beam of ca. 6 pA.
143 Data were collected by rastering a 16 keV primary ion beam of ca. 2 pA Cs^+ focused to a spot size of about 150
144 nm across the sample surface of 40 x 40 μm with a resolution of 256 x 256 pixels and a pixel dwell time of 5
145 ms; except for correlative SEM + NanoSIMS images that were recorded at 55 x 55 μm but not included in the
146 data analysis. The secondary ions $^{12}\text{C}_2^-$, $^{12}\text{C}^{13}\text{C}^-$, $^{12}\text{C}^{14}\text{N}^-$, and $^{12}\text{C}^{15}\text{N}^-$ were simultaneously collected in electron
147 multipliers at a mass resolution of about 9000 (Cameca definition), sufficient to resolve potentially problematic
148 mass interferences. For each sample, seven to eight areas were analyzed in five consecutive image layers. The
149 resulting isotope maps were processed using the ImageJ plug-in OpenMIMS
150 (<https://github.com/BWHCNI/OpenMIMS/wiki>). Mass images were drift- and dead-time corrected, the
151 individual planes were added and $^{13}\text{C}/^{12}\text{C}$ and $^{15}\text{N}/^{14}\text{N}$ maps were expressed as hue-saturation-intensity
152 images, where the color scale represents the isotope ratio. ^{13}C and ^{15}N assimilation was quantified by drawing
153 regions of interest (ROIs) of individual algal symbionts and surrounding host gastrodermis based on $^{12}\text{C}^{14}\text{N}^-$
154 maps. For this, algal symbiont ROIs were drawn by outlining individual algal cells and host ROIs were drawn in
155 a circle with a 15 μm diameter around the centroid of the algal symbiont whilst excluding any algal symbionts
156 and symbiosome content from the ROI. For unlabeled control Aiptasia, 80 host and 80 algal symbiont ROIs
157 were analyzed across two animal replicates. For isotopically labeled Aiptasia, 120 host and 120 algal symbiont
158 ROIs were analyzed across three animal replicates per treatment. Based on this, the ^{13}C and ^{15}N assimilation
159 in individual ROIs was expressed as atom % excess (in comparison to corresponding ROIs of unlabeled control
160 Aiptasia). Due to the clonal nature of Aiptasia and the identical environmental conditions of animals within
161 the same treatment, individual ROIs were considered independent measurements across animal replicates for
162 the purpose of this study.

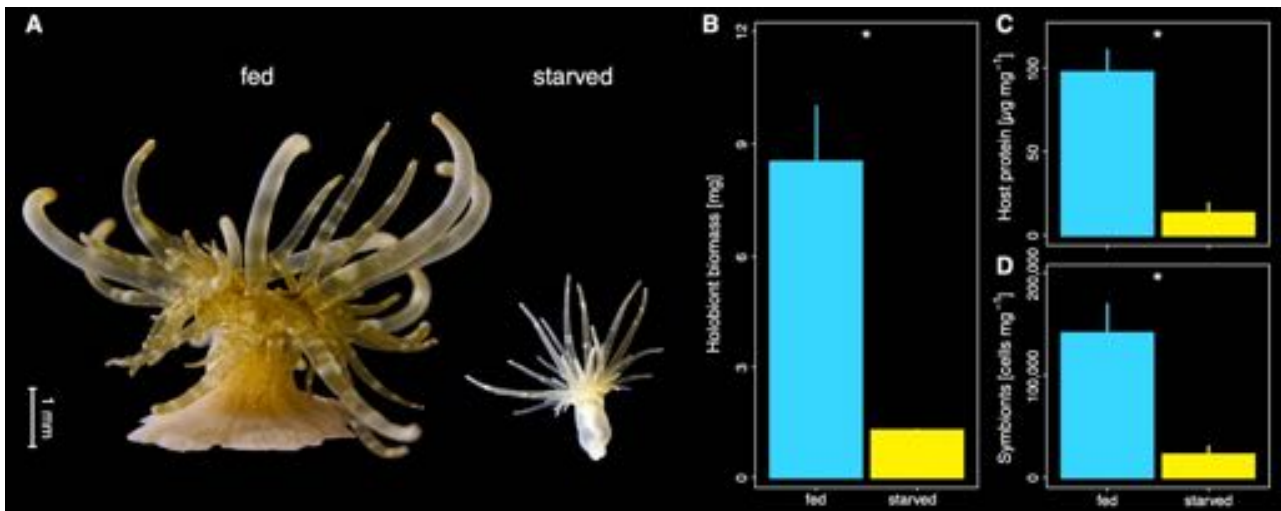
163 *Statistical analyses*

164 Treatment effects on phenotypic responses, i.e., biomass, host protein content, and symbiont density, were
165 analyzed using two-sided unpaired Student's *t*-tests. Isotope ratios from NanoSIMS analysis were log-
166 transformed to meet model assumptions and analyzed with linear models (LM) using the respective symbiotic
167 partner (host/symbiont) and treatment (fed/starved) as explanatory variables. To test individual differences
168 between groups LMs were followed up with a Tukey HSD post hoc comparison.

169 **Results**

170 *Holobiont biomass loss in the absence of heterotrophic nutrients*

171 After one year of husbandry in the absence of heterotrophic food sources, no mortality was observed and
172 Aiptasia remained viable but had ceased any detectable asexual propagation via pedal lacerates. Starved
173 animals showed pronounced phenotypic differences compared to their regularly fed counterparts.
174 Specifically, starvation resulted in a reduction in body size, a paler appearance, and a loss of 85 % of their dry
175 weight (Fig. 1A,B; Student's *t*-test, $t = 4.71$, $p = 0.042$). This decline in holobiont biomass was, at least in part,
176 driven by a strong decline in host protein content and algal symbiont density, which both decreased by more
177 than 80 % on average when normalized to holobiont biomass (Fig. 1C,D; for host protein: Student's *t*-test, $t =$
178 5.39 , $p = 0.014$; for algal symbiont density: Student's *t*-test, $t = 3.85$ $p = 0.047$ for algal symbiont densities).



179

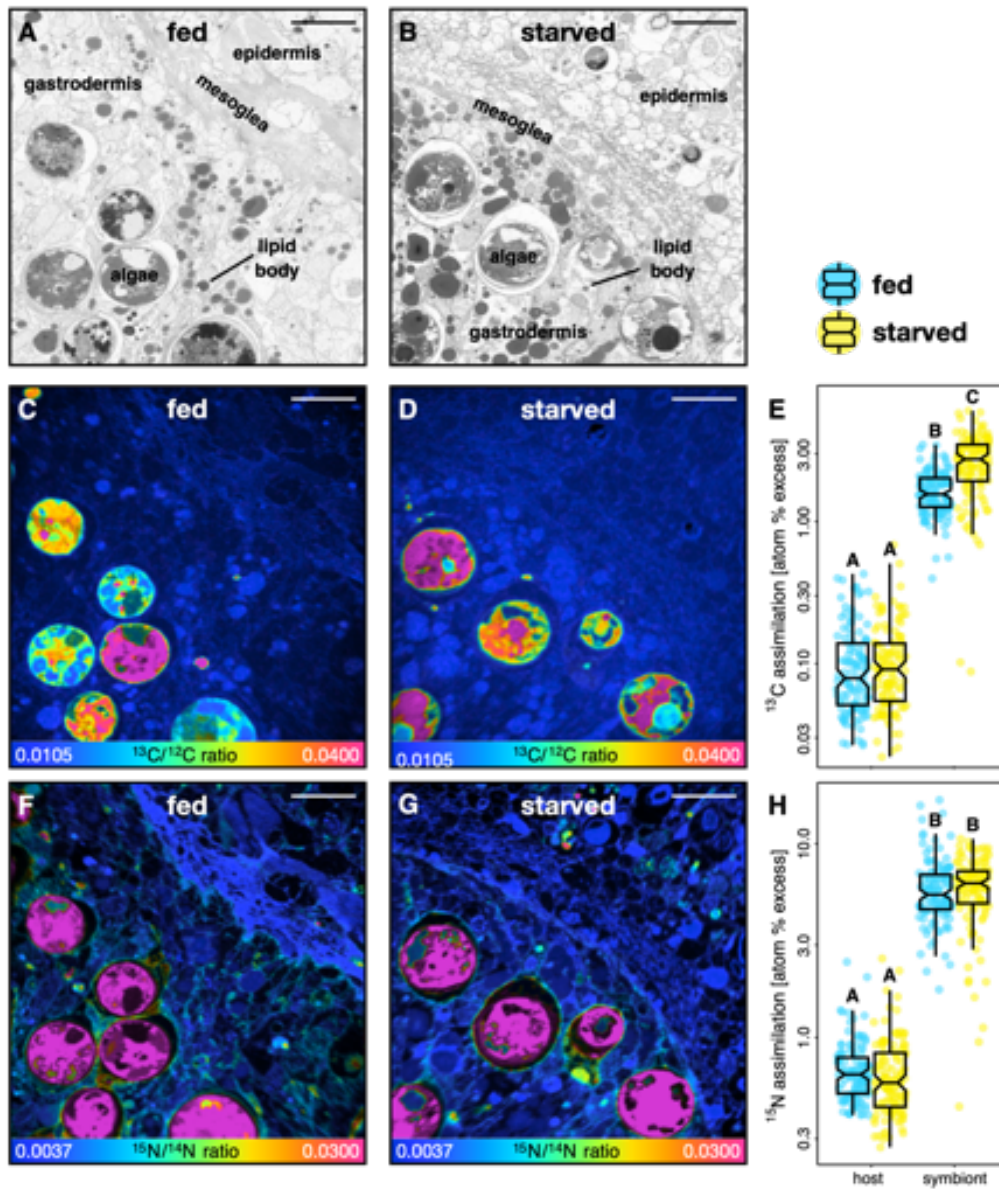
180 **Fig. 1 | Phenotypic response to heterotrophic starvation in Aiptasia.** (A) Representative photos illustrating the phenotype of animals
 181 that were regularly fed (left) or reared for one year without heterotrophic food sources (right). (B) Holobiont biomass expressed as dry
 182 weight of fed and starved Aiptasia. (C) Protein content of the host tissue per holobiont biomass of fed and starved Aiptasia. (D)
 183 Algal symbiont density per holobiont biomass of fed and starved Aiptasia. Three Aiptasia replicates were analyzed for each
 184 treatment. Asterisks indicate significant effects between treatments (* $p < 0.05$).

185 *Enhanced photosynthetic performance of algal symbionts sustains host metabolism during heterotrophic*
 186 *starvation*

187 SEM images of tentacle sections confirmed that Aiptasia from both treatments hosted algal symbionts in their
 188 gastrodermal tissue. However, gastrodermal cells from starved Aiptasia appeared to contain a higher density
 189 of lipid bodies than those of their regular fed counterparts (Fig. 2A,B, Fig. S1). Likewise, algal symbionts from
 190 starved Aiptasia appeared to have a higher lipid content in their cells than those from regularly fed Aiptasia,
 191 albeit this trend was less clear than in the host tissue (Fig. S1).

192 NanoSIMS imaging revealed that metabolic interactions in the cnidarian-algal symbiosis remained remarkably
 193 stable during heterotrophic starvation despite the pronounced phenotypic response of the Aiptasia holobiont.
 194 Consistent with previous reports (Christophe Kopp et al. 2015; Räddecker et al. 2018), the ^{13}C enrichment from
 195 ^{13}C -bicarbonate assimilation/translocation was highest in the algal symbionts with host ^{13}C enrichment
 196 primarily observed in localized hotspots corresponding to lipid bodies in the correlative SEM images (Fig. 2C,D,
 197 Fig. S2; host/symbiont differences: LM, $F = 3189.76$, $p < 0.001$). Despite drastic declines in algal symbiont
 198 densities during heterotrophic starvation, overall ^{13}C enrichment remained stable in the gastrodermal tissue
 199 of the host (Tukey's HSD, $p = 0.951$). This was best explained by the enhanced photosynthetic performance of
 200 algal symbionts, which exhibited an increase of nearly 50 % in ^{13}C enrichment in starved animals (Fig. 2E, Fig.
 201 S2; Tukey's HSD, $p < 0.001$).

202 The constant availability of photosynthates in the symbiosis during heterotrophic starvation was reflected in
 203 a maintained anabolic assimilation of ^{15}N -ammonium by both symbiotic partners. Consistent with previous
 204 studies, the algal symbionts acquired the highest ^{15}N enrichments from ammonium assimilation (Pernice et al.
 205 2012; C. Kopp et al. 2013; Räddecker et al. 2018) (Pernice et al. 2012; Räddecker et al. 2018), but the host also
 206 exhibited clearly measurable ^{15}N enrichments in both epidermal and gastrodermal tissue layers (Fig. 2F,G, Fig.
 207 S2; host/symbiont differences: LM, $F = 3320.37$, $p < 0.001$). Thus, heterotrophic starvation did not alter the
 208 ability for ammonium assimilation of either symbiotic partner (Fig. 2H, Fig. S2; Tukey's HSD, $p = 0.489$ for host
 209 gastrodermis, $p = 1.000$ for algal symbionts).



210

211 **Fig. 2 | Correlative SEM and NanoSIMS imaging of symbiotic carbon and nitrogen cycling in fed and starved Aiptasia.** (A,B)
 212 Representative SEM images of tentacle semi-thin sections of regularly fed and starved Aiptasia, respectively. (C,D) Corresponding
 213 NanoSIMS images illustrating $\text{H}^{13}\text{CO}_3^-$ assimilation and translocation as $^{13}\text{C}/^{12}\text{C}$ isotope ratio maps in regularly fed and starved Aiptasia.
 214 (E) Boxplots and data points of ^{13}C enrichment for the host gastrodermis and the algal symbiont cells. (F,G) Corresponding NanoSIMS
 215 images illustrating $^{15}\text{NH}_4^+$ assimilation as $^{15}\text{N}/^{14}\text{N}$ isotope ratio maps in regularly fed and starved Aiptasia. (H) Boxplots of ^{15}N
 216 enrichment for the host gastrodermis and the algal symbiont cells. NanoSIMS ratio maps are shown as hue saturation images with blue
 217 representing no (or low) enrichment and pink representing the highest level of enrichment. Note the logarithmic scale for E,H. 120
 218 regions of interest across three Aiptasia replicates were analyzed per symbiotic partner and treatment combination. Scale bars are 10
 219 μm . Different letters above boxplots indicate significant differences between groups ($p < 0.05$).

220 Discussion

221 The association with autotrophic endosymbiotic algae has enabled heterotrophic Cnidaria to thrive in the
222 oligotrophic tropical ocean (Muscatine and Porter 1977; Stanley 2006). The long-term starvation experiment
223 presented here emphasizes the remarkable trophic plasticity that such a symbiosis confers upon these
224 cnidarian holobionts. Because of the highly efficient symbiotic nutrient exchange and recycling, Aiptasia were
225 able to survive without heterotrophic feeding for at least one year. At the same time, starved animals showed
226 clear signs of nutrient limitation, including reduced biomass, host protein content, and symbiont density,
227 underscoring the long-term importance of heterotrophic feeding for body mass maintenance and growth.

228 *Autotrophic nutrient recycling can sustain the cnidarian-algal symbiosis for extended periods of time*

229 Recent work suggests that the lack of heterotrophic feeding could shift the cnidarian-algal symbiosis towards
230 parasitic interactions that reduce the capacity of the host to survive starvation (Peng et al. 2020). However,
231 here we show that, even after one year of complete heterotrophic starvation, the translocation of
232 photosynthates by algal symbionts remained sufficient to maintain the basal metabolic requirement of the
233 host. Indeed, patterns of host ^{13}C enrichment (Fig. 2A-C) were not affected by heterotrophic starvation
234 indicating that photosynthate availability for the host was not impaired despite an 85 % reduction in algal
235 symbiont biomass in the holobiont (Fig. 1B). Combined with the pronounced increase in the density of lipid
236 bodies in the host tissue of starved Aiptasia (Fig. S2), this implies that carbon translocation by individual algal
237 cells must have significantly increased in response to heterotrophic starvation. Indeed, we observed a 50 %
238 increase in ^{13}C enrichment and an increased density of lipid bodies among the algal symbionts in starved
239 animals (Fig. 2C), clearly indicating enhanced photosynthetic performance and excess fixed carbon availability
240 required for higher relative translocation rates. Similar, albeit less pronounced, trends were previously
241 reported in a three-month starvation experiment using Aiptasia (Davy and Cook 2001). These authors
242 proposed that the increase in algal photosynthetic performance in starved animals was the result of reduced
243 intra-specific competition for CO_2 . Indeed, reduced algal symbiont densities likely reduce competition for CO_2
244 (Rädecker et al. 2017; Krueger et al. 2020). However, in starved animals, this effect could, in part, be masked
245 by the reduced catabolic CO_2 production in the holobiont due to the lack of heterotrophic prey digestion by
246 the host. Our data point to an additional mechanism that could promote enhanced photosynthate release by
247 algal symbionts in the absence of heterotrophy, namely nitrogen starvation.

248 *Nitrogen limitation shapes the starvation response of Aiptasia*

249 In the stable symbiosis, low nitrogen availability limits the anabolic incorporation of photosynthates in the
250 algal symbiont metabolism (Rädecker et al. 2021; Cui et al. 2022a, 2022b). This nitrogen limitation is thus not
251 only crucial in regulating algal growth but also ensures the translocation of excess photosynthates to the host
252 (Muscatine and Porter 1977; Falkowski et al. 1984). The host passively modulates *in hospite* nitrogen
253 availability for algal symbionts through ammonium assimilation and production of ammonium in its glutamate
254 metabolism (Rahav et al. 1989; Rädecker et al. 2021; Cui et al. 2022a). Here, we found a proportional decline
255 of algal symbiont density and host protein content in heterotrophically starved Aiptasia (Fig. 1C,D). Given that
256 both algal growth and host protein synthesis depend on nitrogen availability this suggests that starvation
257 caused severe nitrogen limitation, which is consistent with previous work documenting increases in the
258 carbon-to-nitrogen ratio and lipid content of Symbiodiniaceae in unfed Aiptasia (Cook et al. 1988; Cook and
259 Muller-Parker 1992; Muller-Parker et al. 1996). Strongly reduced nitrogen availability could thus drive the
260 enhanced translocation of photosynthates by the algal symbionts observed here and explain the long-term
261 survival of Aiptasia during heterotrophic starvation.

262 Interestingly, the reduced nitrogen availability did not cause changes to the ammonium assimilation rates by
263 either symbiotic partner; indeed both continued to efficiently assimilate ammonium from the surrounding
264 seawater in the absence of heterotrophic nutrients. Because ammonium assimilation depends on the
265 availability of carbon backbones from the TCA cycle (Cui et al. 2022b), this observation also suggests that
266 starved holobionts did not experience severe carbon limitation. Yet, the starved holobionts showed severe

267 shrinkage and a significant decline in biomass indicative of malnutrition in the present study. Under the current
268 experimental conditions, environmental ammonium assimilation was thus not sufficient to fulfill the nitrogen
269 requirements of the holobiont. ~~In our experiments, the~~ The availability of seawater ammonium was possibly
270 limited by the rate of water exchange in our experiment (once per week as for the entire animal culture stock).
271 It is thus plausible that higher ammonium concentrations would have allowed the heterotrophically starved
272 Aiptasia to maintain a larger fraction of their original biomass. Yet, in the environmental context of the
273 oligotrophic ocean, photosymbiotic animals are likely similarly limited in their access to environmental
274 ammonium (O’Neil and Capone 2008). In this context, our findings illustrate the importance of heterotrophic
275 feeding by the host for the long-term maintenance of the cnidarian-algal symbiosis biomass. While symbiotic
276 nutrient exchange and recycling may be sufficient to cover the carbon and energy demands of the symbiotic
277 partners on a time scale of at least one year, heterotrophic feeding is not only required for long-term survival
278 but also required for propagation and net growth of the holobiont.

279 Conclusion

280 This study has illustrated the substantial trophic plasticity of the cnidarian-algal symbiosis: Aiptasia survived
281 for an entire year in the complete absence of heterotrophic feeding. Our findings reveal that efficient
282 symbiotic nutrient exchange and recycling are sufficient to sustain the basic metabolic requirements of both
283 symbiotic partners over extended periods of time. Yet, under long-term exposure to highly oligotrophic
284 conditions, the assimilation of environmental inorganic nitrogen is not sufficient to support the nutritional
285 requirements of the holobiont, and heterotrophic feeding represents an essential source of nitrogen for
286 holobiont growth. ~~Under oligotrophic conditions, m~~ Mixotrophy thereby provides a nutritional advantage to
287 photosymbiotic cnidarians that in part explains their ability to outcompete other organisms restricted to either
288 autotrophic or heterotrophic nutrient acquisition under oligotrophic conditions.

289 Acknowledgments

290 We are grateful to Dr. Claudia Pogoreutz and Gaëlle Toullec for their help with animal culture maintenance.
291 We thank Jean Daraspe and Dr. Cristina Martin-Olmos for their help with sample processing and SEM imaging
292 as well as Dr. Stéphane Escrig and Florent Plane for their assistance and support with NanoSIMS
293 measurements. We thank the editor/recommender as well as the two reviewers for their constructive
294 feedback that significantly improved the manuscript.

295 References

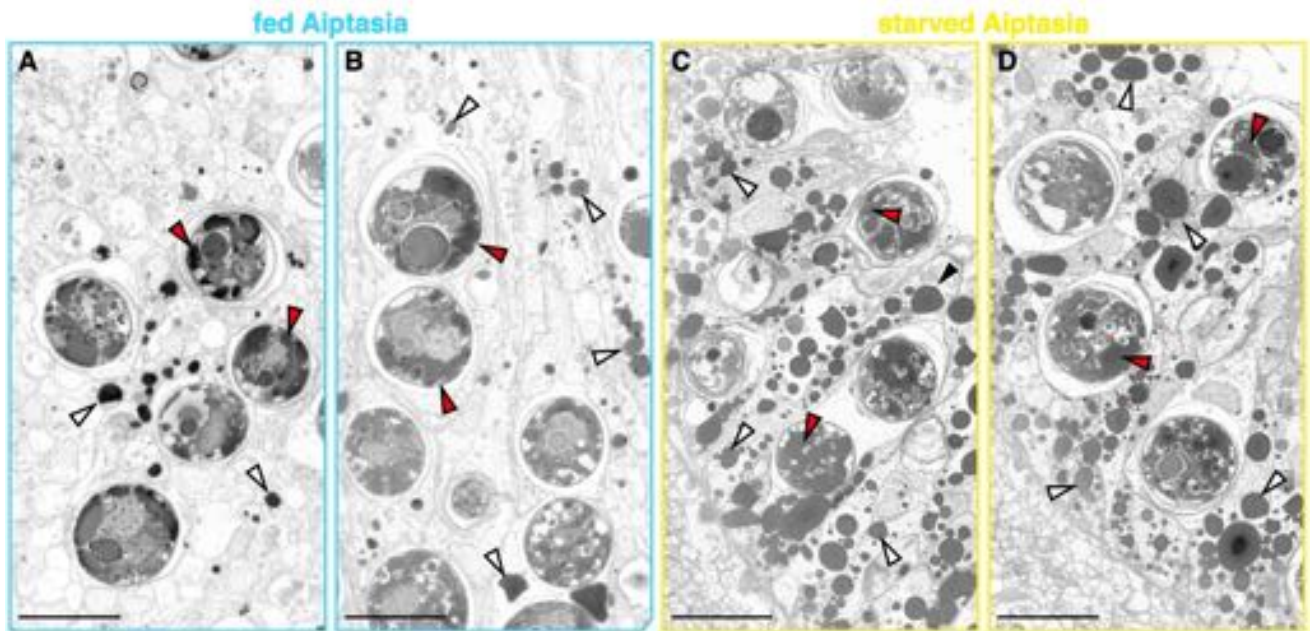
- 296 Anthony KRN, Hoogenboom MO, Maynard JA, Grottoli AG, Middlebrook R (2009) Energetics approach to predicting mortality risk from environmental
297 stress: a case study of coral bleaching. *Funct Ecol* 23:539–550
- 298 Burriesci MS, Raab TK, Pringle JR (2012) Evidence that glucose is the major transferred metabolite in dinoflagellate–cnidarian symbiosis. *J Exp Biol*
299 215:3467–3477
- 300 Cook CB, D’Elia CF, Muller-Parker G (1988) Host feeding and nutrient sufficiency for zooxanthellae in the sea anemone *Aiptasia pallida*. *Mar Biol* 98:253–
301 262
- 302 Cook CB, Muller-Parker G (1992) Ammonium enhancement of dark carbon fixation and nitrogen limitation in symbiotic zooxanthellae: effects of feeding
303 and starvation of the sea anemone *Aiptasia pallida*. *Limnology and* 37:131–139
- 304 Cui G, Liew YJ, Konciute MK, Zhan Y, Hung S-H, Thistle J, Gastoldi L, Schmidt-Roach S, Dekker J, Aranda M (2022a) Nutritional control regulates symbiont
305 proliferation and life history in coral-dinoflagellate symbiosis. *BMC Biol* 20:103
- 306 Cui G, Mi J, Moret A, Zhong H, Hung S-H, Al-Babili S, Aranda M (2022b) Nitrogen competition is the general mechanism underlying cnidarian-
307 Symbiodiniaceae symbioses. *bioRxiv* 2022.06.30.498212
- 308 Cunning R, Muller EB, Gates RD, Nisbet RM (2017) A dynamic bioenergetic model for coral-*Symbiodinium* symbioses and coral bleaching as an alternate
309 stable state. *J Theor Biol* 431:49–62
- 310 Davies PS (1984) The role of zooxanthellae in the nutritional energy requirements of *Pocillopora eydouxi*. *Coral Reefs* 2:181–186
- 311 Davy S, Cook C (2001) The relationship between nutritional status and carbon flux in the zooxanthellate sea anemone *Aiptasia pallida*. *Mar Biol* 139:999–
312 1005
- 313 Dubinsky Z, Jokiel PL (1994) Ratio of energy and nutrient fluxes regulates symbiosis between zooxanthellae and corals. *Pacific Science* 48:313–324

- 314 Falkowski PG, Dubinsky Z, Muscatine L, Porter JW (1984) Light and the bioenergetics of a symbiotic coral. *Bioscience* 34:705–709
- 315 Fox MD, Williams GJ, Johnson MD, Radice VZ, Zgliczynski BJ, Kelly ELA, Rohwer FL, Sandin SA, Smith JE (2018) Gradients in primary production predict
316 trophic strategies of mixotrophic corals across spatial scales. *Curr Biol* 28:3355–3363.e4
- 317 Goreau TF, Goreau NI, Yonge CM (1971) Reef corals: autotrophs or heterotrophs? *Biol Bull* 141:247–260
- 318 Grawunder D, Hambleton EA, Bucher M, Wolfowicz I, Bechtoldt N, Guse A (2015) Induction of gametogenesis in the cnidarian endosymbiosis model
319 *Aiptasia* sp. *Sci Rep* 5:15677
- 320 Grottoli AG, Rodrigues LJ, Palardy JE (2006) Heterotrophic plasticity and resilience in bleached corals. *Nature* 440:1186–1189
- 321 Hambleton EA, Jones VAS, Maegele I, Kvaskoff D, Sachsenheimer T, Guse A (2019) Sterol transfer by atypical cholesterol-binding NPC2 proteins in coral-
322 algal symbiosis. *Elife* 8:
- 323 Harrison PJ, Waters RE, Taylor FJR (1980) A broad spectrum artificial sea water medium for coastal and open ocean phytoplankton. *J Phycol* 16:28–35
- 324 Hoppe P, Cohen S, Meibom A (2013) NanoSIMS: Technical aspects and applications in cosmochemistry and biological geochemistry. *Geostandards and*
325 *Geoanalytical Research* 37:111–154
- 326 Houlbrèque F, Ferrier-Pagès C (2009) Heterotrophy in tropical scleractinian corals. *Biol Rev Camb Philos Soc* 84:1–17
- 327 Hughes AD, Grottoli AG, Pease TK, Matsui Y (2010) Acquisition and assimilation of carbon in non-bleached and bleached corals. *Mar Ecol Prog Ser*
328 420:91–101
- 329 Kopp C, Domart-Coulon I, Escrig S, Humbel BM, Hignette M, Meibom A (2015) Subcellular investigation of photosynthesis-driven carbon
330 assimilation in the symbiotic reef coral *Pocillopora damicornis*. *mBio* 6: e02299-14
- 331 Kopp C, Pernice M, Domart-Coulon I, Djediat C, Spangenberg JE, Alexander DTL, Hignette M, Meziane T, Meibom A (2013) Highly
332 dynamic cellular-level response of symbiotic coral to a sudden increase in environmental nitrogen. *mBio* 4: e00052-13 Krueger T,
333 Horwitz N, Bodin J, Giovani M-E, Escrig S, Fine M, Meibom A (2020) Intracellular competition for nitrogen controls dinoflagellate population density
334 in corals. *Proc Biol Sci* 287:20200049
- 335 McCook L (2001) Competition between corals and algal turfs along a gradient of terrestrial influence in the nearshore central Great Barrier Reef. *Coral*
336 *Reefs* 19:419–425
- 337 Morris LA, Voolstra CR, Quigley KM, Bourne DG, Bay LK (2019) Nutrient Availability and Metabolism Affect the Stability of Coral–Symbiodiniaceae
338 Symbioses. *Trends Microbiol* 27:678–689
- 339 Muller-Parker G, Lee KW, Cook CB (1996) Changes in the ultrastructure of symbiotic zooxanthellae (*Symbiodinium* sp., Dinophyceae) in fed and starved
340 sea anemones maintained under high and low light. *Journal of Phycology* 32:987–994
- 341 Muscatine L, Porter JW (1977) Reef corals: mutualistic symbioses adapted to nutrient-poor environments. *Bioscience* 27:454–460
- 342 O’Neil JM, Capone DG (2008) Nitrogen cycling in coral reef environments. *Nitrogen in the marine environment*. Elsevier New York, pp 949–989
- 343 Pandolfi J (2002) Coral community dynamics at multiple scales. *Coral Reefs* 21:13–23
- 344 Peng S-E, Moret A, Chang C, Mayfield AB, Ren Y-T, Chen W-NU, Giordano M, Chen C-S (2020) A shift away from mutualism under food-deprived
345 conditions in an anemone-dinoflagellate association. *PeerJ* 8:e9745
- 346 Pernice M, Meibom A, Van Den Heuvel A, Kopp C, Domart-Coulon I, Hoegh-Guldberg O, Dove S (2012) A single-cell view of ammonium assimilation in
347 coral–dinoflagellate symbiosis. *ISME J* 6:1314–1324
- 348 Porter JW (1976) Autotrophy, heterotrophy, and resource partitioning in Caribbean reef-building corals. *Am Nat* 110:731–742
- 349 Puntin G, Sweet M, Fraune S, Medina M, Sharp K, Weis VM, Ziegler M (2022) Harnessing the power of model organisms to unravel microbial functions
350 in the coral holobiont. *Microbiol Mol Biol Rev* e0005322
- 351 Rådecker N, Meibom A (2022) Data for “Symbiotic nutrient cycling enables the long-term survival of *Aiptasia* in the absence of heterotrophic food
352 sources.”
- 353 Rådecker N, Pogoreutz C, Gegner HM, Cárdenas A, Roth F, Bougoure J, Guagliardo P, Wild C, Pernice M, Raina J-B, Meibom A, Voolstra CR (2021) Heat
354 stress destabilizes symbiotic nutrient cycling in corals. *Proc Natl Acad Sci U S A* 118: e2022653118
- 355 Rådecker N, Pogoreutz C, Wild C, Voolstra CR (2017) Stimulated Respiration and Net Photosynthesis in *Cassiopeia* sp. during Glucose Enrichment
356 Suggests in hospite CO₂ Limitation of Algal Endosymbionts. *Front Mar Sci* 4:16
- 357 Rådecker N, Raina J-B, Pernice M, Perna G, Guagliardo P, Kilburn MR, Aranda M, Voolstra CR (2018) Using *Aiptasia* as a model to study metabolic
358 interactions in cnidarian-*Symbiodinium* symbioses. *Front Physiol* 9:214
- 359 Radice VZ, Brett MT, Fry B, Fox MD, Hoegh-Guldberg O, Dove SG (2019) Evaluating coral trophic strategies using fatty acid composition and indices.
360 *PLoS One* 14:e0222327
- 361 Rahav O, Dubinsky Z, Achituv Y, Falkowski PG, Smith DC (1989) Ammonium metabolism in the zooxanthellate coral, *Stylophora pistillata*. *Proceedings*

- 362 of the Royal Society of London B Biological Sciences 236:325–337
- 363 Rinkevich B (1989) The contribution of photosynthetic products to coral reproduction. *Mar Biol* 101:259–263
- 364 Stanley GD Jr (2006) Photosymbiosis and the evolution of modern coral reefs. *Science* 312:857–858
- 365 Stanley GD, van de Schootbrugge B (2009) The evolution of the coral–algal symbiosis. In: van Oppen M.J.H., Lough J.M. (eds) *Coral bleaching: patterns, processes, causes and consequences*. Springer Berlin Heidelberg, Berlin, Heidelberg, pp 7–19
- 367 Sunagawa S, Wilson EC, Thaler M, Smith ML, Caruso C, Pringle JR, Weis VM, Medina M, Schwarz JA (2009) Generation and analysis of transcriptomic resources for a model system on the rise: the sea anemone *Aiptasia pallida* and its dinoflagellate endosymbiont. *BMC Genomics* 10:258
- 368
- 369 Tremblay P, Grover R, Maguer JF, Hoogenboom M, Ferrier-Pagès C (2014) Carbon translocation from symbiont to host depends on irradiance and food availability in the tropical coral *Stylophora pistillata*. *Coral Reefs* 33:1–13
- 370
- 371 Tremblay P, Grover R, Maguer JF, Legendre L, Ferrier-Pagès C (2012) Autotrophic carbon budget in coral tissue: a new ¹³C-based model of photosynthate translocation. *J Exp Biol* 215:1384–1393
- 372
- 373 Yellowlees D, Rees TAV, Leggat W (2008) Metabolic interactions between algal symbionts and invertebrate hosts. *Plant Cell Environ* 31:679–694

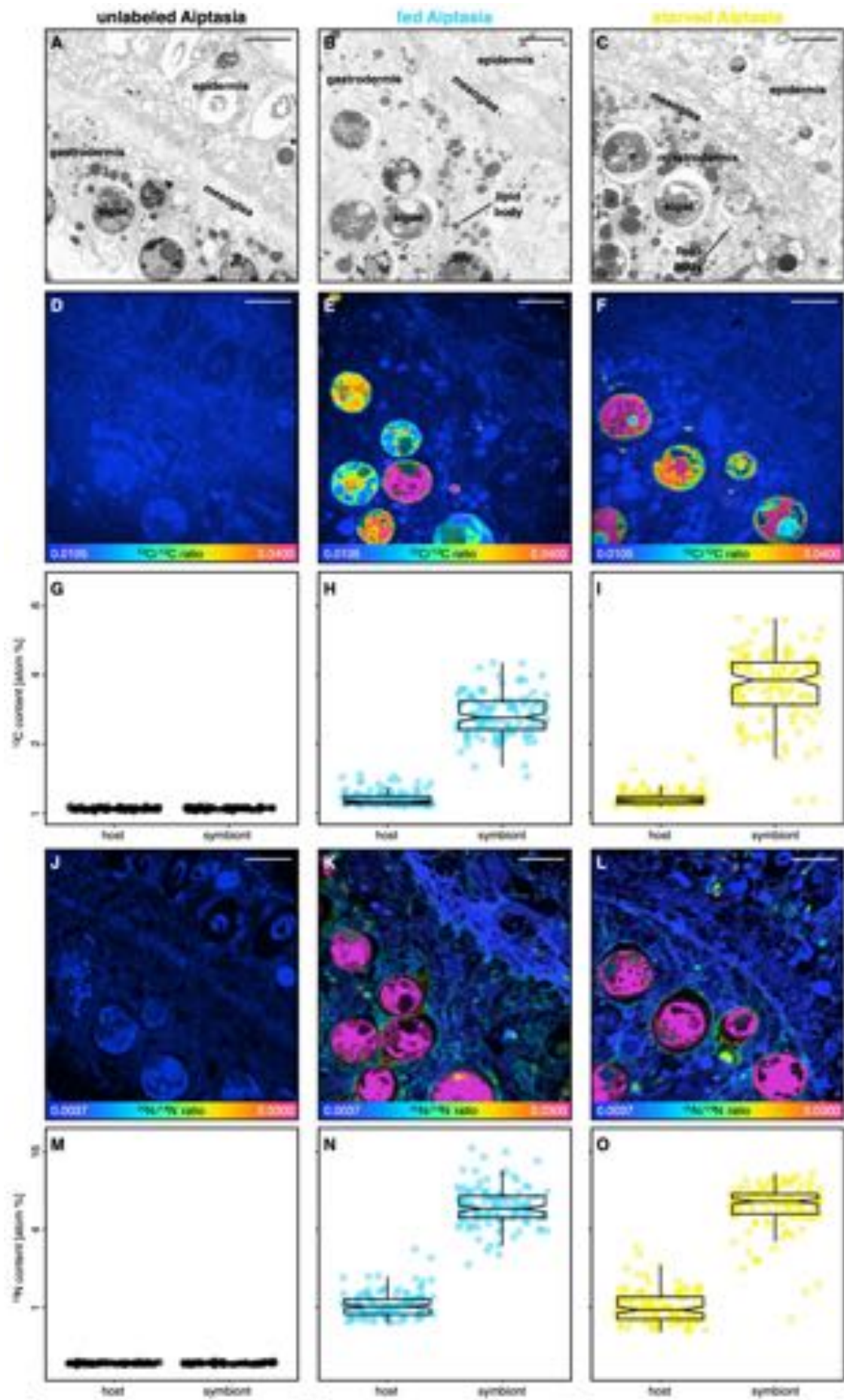
374
375
376
377
378

Supplementary material
for
“Symbiotic nutrient cycling enables the long-term survival of *Aiptasia*
in the absence of heterotrophic food sources”



379

380 Fig. S1 | SEM images of semi-thin sections of gastrodermal regions of tentacles from (A,B) regularly fed and (C,D) starved *Aiptasia*.
381 White triangles point to lipid bodies in the host gastrodermis; red triangles point to lipid bodies in the algal symbionts. Scale bars are
382 10 μ m.



384 **Fig. S2 | Correlative SEM and NanoSIMS imaging of symbiotic carbon and nitrogen cycling in unlabeled, fed, and starved Aiptasia.**
385 **(A-C)** Representative SEM images of tentacle semi-thin sections of unlabeled, regularly fed and starved Aiptasia, respectively. **(D-F)**
386 Corresponding NanoSIMS images illustrating $\text{H}^{13}\text{CO}_3^-$ assimilation and translocation as $^{13}\text{C}/^{12}\text{C}$ isotope ratio maps. **(G-I)** Boxplots and
387 data points of ^{13}C content for the host gastrodermis and the algal symbiont cells. **(J-L)** Corresponding NanoSIMS images illustrating
388 $^{15}\text{NH}_4^+$ assimilation as $^{15}\text{N}/^{14}\text{N}$ isotope ratio maps. **(M-O)** Boxplots of ^{15}N enrichment for the host gastrodermis and the algal symbiont
389 cells. NanoSIMS ratio maps are shown as hue saturation images with blue representing no/low enrichment and pink representing the
390 highest level of enrichment. Note the logarithmic scale for **G-I** and **M-O**. Scale bars are 10 μm . For the unlabeled Aiptasia, 80 regions
391 of interest across two Aiptasia replicates were analyzed. For the other treatments, 120 regions of interest across three Aiptasia
392 replicates were analyzed per symbiotic partner.